A neural network-based low-cost soft sensor for touch recognition and deformation capture

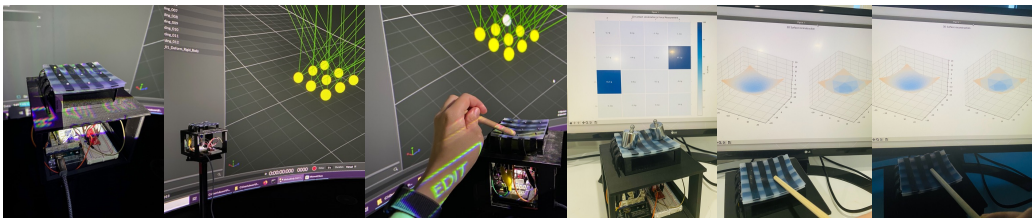

Fig. 1. Our low-cost soft sensor detects contact areas, measures force, and reconstructs 3D virtual sensor surfaces in real-time. It identifies both single and multiple contact points and can reflect surface deformation in a dark environment.

We present a stretchable, low-cost soft sensor that can detect contacting force, single and multiple touching areas, and reflect the sensor deformation with a 3D virtual surface in real-time, all without the use of optical devices. Our capacitive stretchable sensor is fabricated using only inexpensive materials, a 3D printer, laser cutter, and other simple equipment. Our sensor also uses trained neural network models to translate the signal directly into the localization, force measurement, and out-of-sight deformation. We propose an effective data collection system that captures ground-truth 2D localization, force measurements, and 3D surface geography data and generates a high-quality, pre-validated data set. The data set is fed to two neural network models after it has been filtered using prior knowledge. In a series of controlled experiments, we demonstrate the stability and accuracy of the prototype soft sensor. In both single-point and multi-point contact scenarios, our sensor achieves reliable results.

CCS Concepts: • **Hardware → Sensors and actuators**.

Additional Key Words and Phrases: Soft user interface, capacitive sensor, deformation capture

ACM Reference Format:

. 2022. A neural network-based low-cost soft sensor for touch recognition and deformation capture. 1, 1 (August 2022), 21 pages. https://doi.org/10.1145/nnnnnnn.nnnnnnn

1 INTRODUCTION

For humans and other animals, the skin is one of the most fundamental means of perceiving the environment. No matter if we are shaking hands, touching an object, or being bitten by a fly, our skin allows us to feel contact forces and locate areas of contact. The term, wearable technology, has fueled a boom in wearable devices over the past few years, and soft sensors, which resemble biological skin, have become a hot topic in human-computer interaction. Flexible and stretchable sensors are naturally useful in the fields of robotic arms and human-computer interaction. However, assembling a soft sensor has proven to be challenging and costly. It's mainly due to the fact that the material used for the stretchable sensor is expensive and the fabrication workflow of embedded electrodes typically requires an industrial laboratory.

As illustrated in Figure 1, we present a novel, low-cost soft sensor that can be produced in a typical university laboratory. As part of our efforts to reduce costs and increase stability, we have designed a fabrication workflow that

Author's address:

requires a 3D printer and laser cutter to minimize the level of manual work and complexity of electrode fabrication. Besides, the primary components of our sensor are a shaped carbon nanotube (CNT) sheet and RTV silicone (room-temperature-vulcanizing silicone). The total cost of sensor material is low and we can fabricate the sensor without strictly enforced device specifications. In addition, the connecting hardware of a sensor is typically difficult to design and implement. The cost of the soft sensor could be increased by the readout device. To overcome it, we implemented an Arduino-based data reader. The usage of Arduino boards simplifies hardware design and provides millisecond-accurate readings.

Vision-based systems are exploited for various applications to capture surface deformation in three dimensions. For these solutions, however, motion-tracking cameras, reflective markers, and particular environmental conditions are required. In general, it is difficult to use camera-based applications with wearables and robotic arms due to obscured images and a lack of light. As a sensor-based solution, our prototype sensor is capable of reconstructing pushing deformation in real-time and achieving the same performance in an out-of-sight environment. To accomplish this, our soft sensor combines the capacitance sensor array concept with a data-driven approach. The integrated soft sensor system detects capacitance variations using CNT electrodes. Mixed CNT electrodes and silicone material are flexible and deformable during the touching operation. In the meantime, neural network models are utilized to address the potential relationship between raw sensor signals and expected patterns. This permits us to detect touch location, measure touch force, and capture surface deformation in real-time.

Building a large and efficient data set for a new soft sensor is incredibly hard due to the lack of suitable methods. This study implements a real-time data collection system for gathering ground-truth data. In terms of localization and touching force, we define an output format that includes force value and 2D position to gather the actual data. To capture the surface deformation, we attach small reflective markers to the surface of soft sensors and use motion capture (MoCap) technology to collect the markers' position in real-time. Following the collection of raw data, the data set will be processed via the steps of data cleaning, moving averaging, and coordinate system transformation based on prior knowledge of the geometric position. The converted data reflects the variation of capacitance more accurately.

To verify the precision of the sensor prototype and data sets, we compare the accuracy of 2D localization using different testing scenarios. In the meantime, we examine the accuracy of 3D surface deformation capture using a test data set. Due to its simplified fabrication method and low price, our prototype has the potential to be used in wearable devices and sensing applications.

2 RELATED WORKS

Our work involves a wide range of fields, including deformable input and capacitive sensors. In this section, we briefly review the fundamental works in these fields.

2.1 Deformable input

The research on sensor-based deformation capture and touch recognition have its roots in deformable input [1] [6]. Deformable input devices have primarily been utilized to replace traditional input devices regarding medical devices, controllers and smart mobile devices. Compared to the standard input devices such as the mouse and keyboard, the deformable input device offers a greater variety of shapes and sensing approaches [3]. For instance, the deformable input allows users to control the laptop through an interactive display. Wearable devices can be adapted to assist individuals with disabilities in their day-to-day activities. The fabrication principles of sensors are also diverse. Researchers have explored this domain using various flexible sensors. The majority of deformable inputs are designed to deal with specific

obstacles. Thus, researchers tend to limit the capabilities of these sensors. For instance, Sugiura et al. [54] designed a sensor that can only identify stretching and has minimal use cases. The sensor described in [64] is only utilized to identify concrete cracks.

Research on deformable input devices can be divided into two categories: hand input and body input [39]. Due to the flexibility of human hands, deformable hand input is the focus of most research. Hand input deformation classes include bending, folding, stretching, and pressing, according to [32]. Bending is a common shape change, which often results in displays, handheld controllers [52], and musical instruments [34]. Folding often occurs in mobile phones, monitors, and some specific controllers. Typically, stretching is used in two-handed operations and one-handed stretchable sensors, such as pulling straps. The primary research context for deforming planes, touching screens and pressing sensors is pressing [5] [55] [56] [20].

Early research focused primarily on detecting a single type of deformation, known as one-dimensional deformation. In recent years, scientists have shifted their attention to multidimensional deformation, such as soft body inputs. Body inputs or wearable devices enable researchers to record the deformation of specific body parts using self-sensing devices [23]. For instance, Baldwin et al. [4] identifies the user's gait pattern and predicts whether or not they will fall. Singh et al. [51] categorises body positions. The reference [36] describes a recently developed pressure perception device. Parzer et al. [37] implements a sleeve to differentiate postures from raw data. Huang et al. [19] presents a sensor attached to the elbow that detects elbow movement. The sensor made by Ma et al. [27] can detect leg movement. By detecting the body's electric field with an integrated sensor, Yildirim et al. [65] augments the human body's sensing capabilities.

2.2 Capacitive sensors

Capacitive sensors are associated with the research of human-computer interaction [16]. There are several fundamental characteristics of the capacitive sensor that have caught the attention of researchers. Capacitance sensing, for instance, utilizes only electricity, and the capacitor principle is simple [28]. A capacitive sensor consumes little power and its components are widely accessible and reasonably priced [18] [63]. Prior research has primarily focused on lowering fabrication costs, boosting sensor sensitivity for deformation, and implementing flexible sensors.

Since 1997, capacitance and electrodes have been integrated into touch sensors [23]. Murakami and Nakajima [31] introduced capacitive sensors as the hardware component of deformable input devices in the year 2000. By collecting the capacitance change with the input device, researchers can map the shape change to the capacitance change in the real world. The Sony research team implemented a deformable display utilizing a grid capacitive sensor in 2002 [40]. Changes in capacitance display can identify the location of finger contact. Through this research, occlusion defects caused by vision devices can be avoided. In 2007, researchers proposed a flexible, printed sensor [58]. Because the electrode distribution has been pre-designed, the printed sensor can detect surface deformation. However, it is unable to pinpoint the location of the deformation.

To identify the location of touch and deformation, the researchers developed a microcontroller-based capacitive touch sensor [7]. This sensor is able to detect the precise location of the touch thanks to its 2D mesh structure. However, the sensor area is small and the sensing space is fixed. To bypass the shape restriction, Savage et al. [48] defined a method that can automatically cut the electrode layout based on the design. Copper foil is used to construct the sensor electrode, and a laser cutter is used to automate the cutting process. Such an approach overcomes the limitations of sensor shapes, allowing researchers to modify sizes and layouts to suit their requirements. Nonetheless, the sensor is not

stretchable or foldable, and the copper wire is not durable. Consequently, Grosse-Puppendahl et al. [15] implemented a brand-new motherboard platform to reduce costs and improve robustness, linking up to 8 low-cost sensors.

To open up a path towards a large electrode number, Rus et al. [46] brought up the idea of 2D mesh structures for the electrode layout. Later, Gong et al. [14] reintroduced the printed electrode pattern to increase electrodes. Rendl et al. [41] described another printable electrode layout and sensor structure that significantly expands the number of electrodes and their coverage area. Utilizing the concept of Rendl et al. [41], Rendl et al. [42] proposed a redesigned sensor layout to sense folding. Later, Nguyen et al. [33] achieved a low-cost, flexible interface with new materials. This sensor is composed of conductive foam and fabric and can locate the spot of the deformation on the 3D model. It requires 8 nodes to capture the direction of folding but fails to reflect the deformation's details.

From a different angle, Mehmann et al. [29] implemented a flexible input with 56 electrodes and attempted to capture the shape of the bump layout. In 2015, Schmitz et al. [49] embedded conductive carbon-based materials into 3D-printed models. The shape of the conductive materials can be flexible. In the same year, Weigel et al. [60] designed a novel type of flexible sensor that allows users to design the shape and size of the sensor with laser cutting. The capacitive circuit is composed of cPDMS (carbon doped polydimethylsiloxane), and the laser cutter can also be used to shape the layout of cPDMS. Although the sensor can only detect the pressing and not the location of the contact, its design has inspired future research such as [22]. After that, a new elastic and flexible electrode material was developed [2]. In this work, the fabrication complexity of capacitive sensors was reduced by automating the workflow. Casting materials, laser-patterning electrodes, and applying a protective layer consists of the standard fabrication process. PVA (Polyvinyl alcohol) is used to adhere the circuit to the surface of PDMS (Polydimethylsiloxane), which simplifies the production workflow.

To enlarge the scale of the sensing area, Roudaut et al. [44] proposed a modular deformable sensor. As a solution to the material cost limitation, Yoon et al. [66] developed a cost-effective real-time detection sensor with conductive silicone rubber. Instead of grid electrodes, they applied the Neighboring Method to track the location of the deformation. The downside of the neighboring method is that accuracy will decrease during stretching. Yoon et al. [67] also used Neighboring Method, but they decided to use a machine learning algorithm to process the collected data and achieved positive results.

2.3 Fabrication

Initial research directions for fabrication are concentrated on material breakthroughs. Sensor performance is typically improved by increasing the conductivity and flexibility of the materials. As a result of the invention of novel materials, the workflow for fabricating objects becomes heavily complicated, and the price tends to increase vastly. For instance, Sekitani et al. [50] provided SWNT-based (Single-Wall Carbon Nanotubes) stretchable conductors. Thus, the fabrication process requires a high-pressure jet-milling homogenizer and the continuous addition of various materials to the gel. It has restrictive temperature and time requirements.

To reduce the complexity, researchers proposed various solutions with cheap materials. Grosse-Puppendahl et al. [15] described the motherboard and the sensor link. Wikström et al. [62] utilized the conductive tape to perform sensing. Grosse-Puppendahl et al. [16] introduced wires and sheets to construct the sensor. Although these sensors reduced costs, the sensor materials are not standardized, and each solution has a unique fabrication process. And therefore, the production process necessarily requires a fair bit of manual work, resulting in a massive influence on sensor precision.

Over the years, scientists have invented automated fabrication using cutting machines and automatic printing mechanisms. Through the use of cutting machines, Savage et al. [48] achieved flexible copper circuits. Gong et al. [14]

designed an automated manufacturing process that prints the layout of copper electrodes. Kao et al. [22] produced the circuit layout by slicing the gold leaf. Peng et al. [38] designed and implemented a new type of 3D printer, which is capable of printing deformable and complex objects directly. Besides this, it can also print multilayer circuits. The printed model, however, is relatively rough. Araromi et al. [2] described a flexible and stretchable single-layer electrode circuit material, and most of the processes were automated. This stretchable material's substrate is composed of PDMS. PVA plane is formed by casting, and during fabrication, unshaped electrode layers are covered with screening on the PVA plane. The circuit is then printed via laser patterning. Wessely et al. [61] used UV lithography to print the sensing area. Rosset et al. [43] presented a fabrication approach in which the stretchable film was attached to the placeholder and printed by machines. By 3D printing a sensor mold and squeegeeing conductive ink, Jeong and Lim [21] minimized the amount of manual work.

In addition, screen printing can also be achieved through shadow masks [50]. Later, Cholleti et al. [8] described a novel method for simultaneously printing conductive ink and conductor material. Yoon et al. [66] mixed the nano-titanium tube material with other substances to make a flat surface. During the manufacturing process, they utilized a heat press and toast oven to accelerate the curing. Unlike the previous production process, this fabrication workflow can be re-implemented in the laboratory setting. Yoon et al. [67] also strived to use the toast oven in the production process. However, the electrodes of the above-mentioned sensor types only consist of a single layer. Moreover, researchers have integrated laser cutters into fabrication steps in an attempt to streamline production [27] and inspired our work.

2.4 Analysis approach

The analysis approach of capacitive sensors is closely related to the sensor layout. The simplest electrode layout involves positioning the sensor at a predetermined location and capturing touch or deformation via sensor data changes at each predetermined location. The approach described by Grosse-Puppendahl et al. [15] involves the placement of up to eight touch sensors in a predetermined scene. Lissermann et al. [26] developed a wearable ear device that can respond to both single and possible multiple touches. The device can be used as a controller for playing music, adjusting the volume, and pausing the music by touching the predefined sensing area. Wikström et al. [62] provided conductive tape with motionless electrodes. Thus, only a few deformations can be gathered. Additionally, the wearable sensor provided by Singh et al. [51] has fixed electrode positions. Parzer et al. [36] used rows electrode to measure pressure. Sarwar et al. [47] proposed the grid sensor array to identify the location of the touch. Han et al. [17] designed a deformable flexible plane with linear hall sensors and permanent magnets that can reflect the touch on the plane of a virtual environment in real-time. Through marker detection and camera-based prior knowledge, Rendl et al. [42] achieved the real-time correspondence between the 3D plane and the sensor plane in [33] constructed a virtual 3D model that includes eight pre-installed nodes.

Algorithms and techniques for machine learning and deep learning open up a path to map raw data to corresponding deformations. Cohn et al. [9], for instance, employs KNN (k-nearest neighbors) to map the raw data collected by wearable devices across multiple body actions. Yoon et al. [66] analyzed the deformation and movement collected by the Neighboring Method through linear regression. As a classic algorithm of machine learning, SVM (support vector machine) is also used. Cohn et al. [10] utilized SVM to map electronic noise to various pose classifications. Nguyen et al. [33] identified the direction of the deformation correctly by SVM. Parzer et al. [37] designed a sleeve sensor to collect posture-related deformation and determine the correct posture through SVM. SVM also works well with NeighboringMethod [67].

The problem of identifying the touch position was also viewed as a regression problem by researchers [25]. Thus, they adopted the random decision tree forest to process the regression calculation. Rus et al. [45] opted to use a decision tree to analyze the original data and obtained positive results. After that, Vega et al. [59] identified the subconscious movement through the decision tree. Singh et al. [51] implemented a wearable device to recognize body posture with decision trees. Mohd Noor et al. [30] utilized PCA to reduce the dimensionality of the original data and introduced the Gaussian Process Regression model to predict finger movement. Larson et al. [24] built a grid-like electrode distribution sensor and analyzed the raw data through CNN (convolutional neural network) to identify the touch position in real-time. CNN is additionally mentioned in [12] and [13] and perform positive results.

3 SENSOR DESIGN AND FABRICATION

Our goal is to construct a flexible, low-cost sensor that can be assembled in an university laboratory and is fairly accurate. The majority of current research on soft sensors concentrates on industrial-grade sensing systems. This requires a high level of production environment and is difficult to replicate; the sensor itself is also expensive. Even for flexible sensors that can be assembled in a laboratory, the replication success rate is commonly limited by the necessary equipment. For instance, when combining carbon nanotube material with liquid silicone, the strength and power of the stirrer is essential. Without the proper stirrer, creating materials with uniform conductivity is difficult. In addition, the temperature required to accelerate the solidification of silicone is extremely demanding. If the temperature is too high and air bubbles remain in the silicone, the bubbles will expand during the heating process. An air-filled silicone liquid is incapable of forming a flat surface. In addition, we wish to minimise the manual labour involved in the production process. The success rate of manual production is difficult to guarantee. To improve the quality of the flexible sensors, we would like to use automated machines.

Figure 2 illustrates the final prototype sensor. Our flexible sensors are composed primarily of silicone and have a translucent appearance overall. On the surface of the sensor, the distribution of electrodes and conducting circuits can be observed. Our sensors' primary component is a low-cost material. Each flexible sensor costs less than 14 USD, excluding the 3D-printed support frame and electronics, and has a total thickness of fewer than 4 millimeters. There are extensions on both sides for connecting the circuits to the data reader. Currently, the dimensions of our flexible sensors are 9 cm by 9 cm. When reading the data, our sensors can be self-calibrated and begin outputting capacitance data in less than three seconds. The data reading frequency is measured by microseconds. No additional equipment is required for the setup process. We introduce 3D printers and laser cutters into the fabrication workflow, which greatly reduces the complexity and cost.

3.1 Multi-Layer Structure

As shown in Figure 2, Our soft sensors have a five-layer structure consisting of two protective layers, one dielectric layer and two conductive layers. The dielectric layer is made of the same material as the protective layer and consists of silicone RTV 4420 components [11]. The mixing of RTV silicone requires solvents. We used Toulon and isopropyl alcohol according to the previous research specification [12]. The conductive layers are not all conductive, but have electrodes and circuits embedded in them. The circuitry is made up of CNT sheets. The main components are RTV 230 silicone [57] and TUBALL MATRIX 601 [57]. The CNT sheet is stretchable and deformable and the volume resistivity of the conductive sheet is 1.10$\hat{2}$ Ω.cm. The size of the conductive sheet is 0.14m * 0.14m and the thickness is 2mm. Each sheet has 0.045 kg. We chose these materials due to their low cost and ability to be assembled at room temperature without complex assembly requirements.

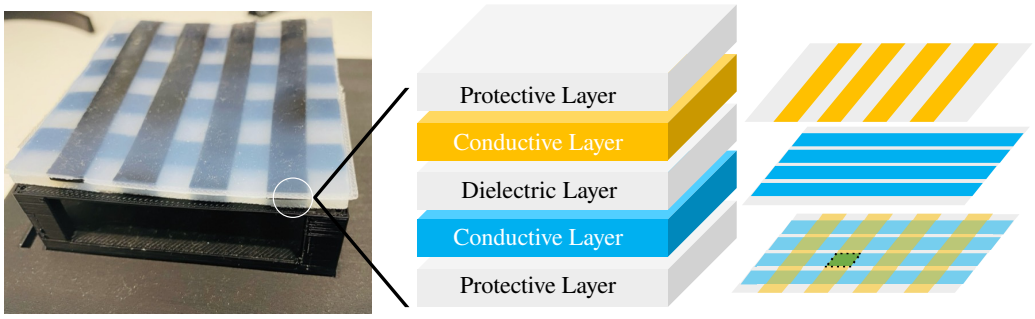

Fig. 2. Left: A prototype soft sensor. Middle: A five-layer structure for the soft sensor. During deformation, the distance between two conductive layers changes, causing a variation in capacitance. Right: Circuits are embedded within each conductive layer. The parts that overlap function as electrodes for our soft sensor.

The two conductive layers have different directions of circuit distribution. When the different layers of the entire flexible sensor are stacked together, the circuit distributions of the different conductive layers intersect in the vertical direction. These intersection points are the electrodes of the flexible sensor. Our flexible sensors recognise the position and intensity of a touch by the change in capacitance of these electrodes. As the different layers of material are stretchable and deformable, our sensors as a whole are also stretchable, deformable and foldable. Our capacitive sensor is a capacitive shape-changing sensor; consequently, the capacitance value of the sensor capacitor is not fixed. The capacitance value of a shape-changing capacitor is determined by the overlapping area of the two electrodes and their distance. During deformation, the distance between the upper and lower electrodes varies, as does the area of overlap. By measuring the real-time change in capacitance, our sensors determine the location and extent of deformation.

The electrode of the current sensor is arranged in a grid pattern. The circuits of the conductive layer cross naturally to form 16 electrodes. The primary purpose of a grid layout is to simplify the process of accessing data and 2D coordinates can be used to position the electrodes in a grid layout. This facilitates the visualization of raw data when reading it. Additionally, the grid layout simplifies data collection. When data is collected from the weight map, the grid layout allows for direct correspondence between the weight map and electrode positions. Besides, the reflection markers were used to collect 3D geographic data and the grid layout of the reflective markers can be matched to that of the electrodes. It makes the validation of the dataset easier.

3.2 Hardware

The data reader is primarily composed of an Arduino motherboard, a multiplexer, and a 3D-printed frame. Utilizing the Arduino motherboard as the prototype's hardware significantly reduces production costs. The data reader's primary function is to rapidly measure the current capacitance of each electrode. During capacitance measurements, the multiplexer is able to swiftly switch between circuit channels. As illustrated in the Figure 3, the data reader measures the current capacitance of the electrodes through the red channel S. When the red channel is connected, the Arduino board records the amount of time required for the capacitance of the electrodes to fill with the current voltage. The data reader's processing time can be used to calculate the electrode's current capacitance. As soon as the output is completed, the multiplexer switches to the next channel. This procedure is repeated until the entire reading is complete. In the invariant state, the entire capacitance of the electrodes can be read in approximately 0.5 microseconds. In a state

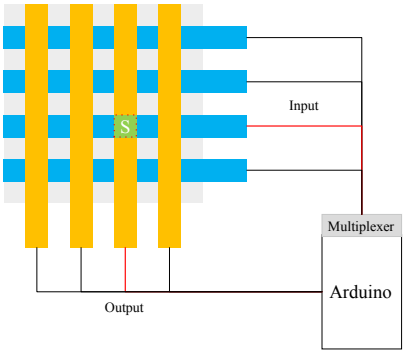

Fig. 3. Capturing the capacitance value S of the sensor electrode that is activated. The data reader is composed of an Arduino board and a multiplexer. After activating the red circuit, the reader is able to collect the value S. By switching multiplexer channels, the capacitance of each electrode is obtained.

of deformation, the total time alters to around 0.9 microseconds. The script installed on the Arduino board keeps track of the current electrode coordinates, capacitance value, and timestamp automatically.

3.3 Fabrication process

As described in Figure 4, the manufacturing procedure is comprised of two distinct workflows. Initially, the conductive layer with the designed electrode layout is produced. In this step, a laser cutter is used to reduce the number of manual operations. The design of the electrode layout is based on the capacitive principle and the CNT sheet is cut with a predetermined electrode layout by the laser machine. Due to the thickness, color, and composition of the CNT sheet, laser cutting must be repeated multiple times along the same cutting path. There is a possibility that the cut electrodes will adhere to the base because of the laser cutter's high temperature. The cut electrode should be cleaned with water and a towel before it can be utilized to create conductive layers.

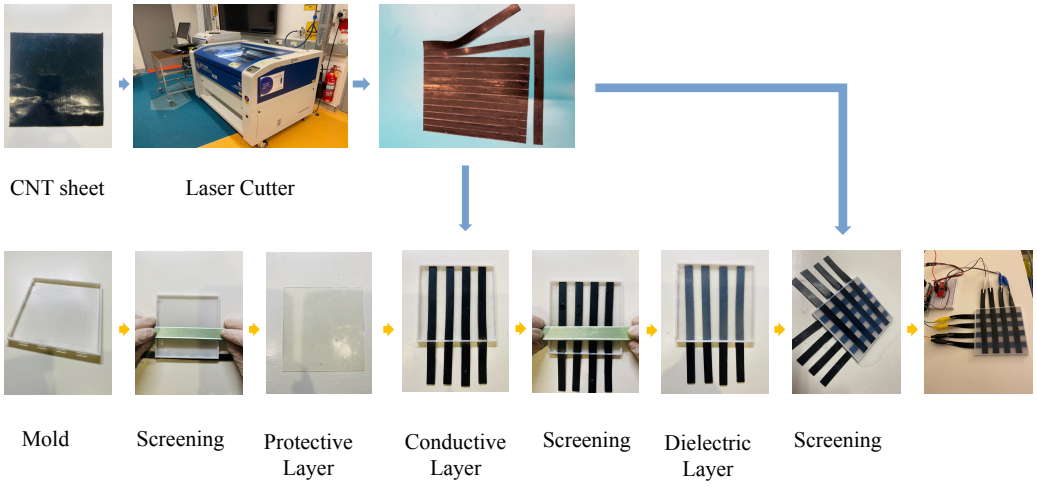

Fig. 4. The fabrication of a soft sensor involves two pipelines: the upper one is for laser-cutting conductive layers and the lower one is for fabricating the multi-layer sensor.

Prior to carrying out the second step, we prepare the sensor molds with a 3D printer. PloyCarb was applied as the printing material on a Stratasys 450mc 3D printer [53] and both sides of the mold were left with extended circuit interfaces. RTV 4420 is the main component of silicone. The silicone liquid requires an equal mixture of RTV 4420 component A and component B. The liquid silicone is difficult to stir and contains numerous air bubbles after mixing. Therefore, additional co-solvents are required for the fabrication process. First, we will combine RTV 4420 component A with Toulon in equal proportions. The mixture will be stirred by hand for five minutes. After stirring the mixture, 1.5 parts of isopropyl alcohol and 1 part of component B are added. The final step is manual stirring for 10 minutes. After stirring, the mixture is clear and devoid of air bubbles.

Following Figure 4, We construct a protective layer. The protective layer is the lowest layer of the soft sensor and is made entirely of silicone. As a protective layer, the liquid silicone is injected into the mold. Using a squeegee, the extra silicone liquid should be removed from the mold. After undergoing natural curing, the silicone within the mold forms a protective layer and its thickness is one millimeter.The protective layer is then positioned within the mold of the dielectric layer.On top of the protective layer, the previously generated electrode layout is positioned and the electrodes' ends can protrude from the mold. After that, we refill the mold with the silicone mixture and squeeze out any extra liquid. After the natural cooling, the first conductive and dielectric layers are formed. The current sensor will be placed in the mold by repeating the preceding steps. After constructing the last protective layer, the flexible sensor is fully functional. Due to the presence of co-solvents, it is critical to note that the silicone solution mixture will emit toxic volatile gases during natural curing. The laboratory containing prototype sensors must be adequately ventilated. The resulting sensor has a thickness of 5 mm and is extensible and deformable. As soon as the sensor has been formed, a data reader is utilized for rapid verification. Ensure that the capacitance data of each electrode is read.

4 DATA ACQUISITION

We employ a data-driven method to detect touch and three-dimensional reconstruction. Consequently, the key to success is the rapid collection and creation of a large and reliable data set. Our sensor solution is, however, a novel product. This indicates that no ready-made data set is available for use and we were required to develop a workflow for data collection from scratch. This workflow requires the ability to rapidly collect relevant data and validate its accuracy. The data set should contain the least amount of possible noise. This is performed to guarantee the accuracy of the model during the following deep learning training. Besides, we want the flexible sensor to detect two-dimensional touch and reconstruct the three-dimensional deformation of a plane. As a result, our data collection workflow is separated into two-dimensional touch sampling and three-dimensional deformation sampling.

4.1 2D Touch Sampling

As shown in Figure 5, we prepare a supporting framework for 2D touching. The sensor is suspended in the middle of the framework and the edges of the sensor are attached to the frame. We detect the position and force of contact using calibration weights. There are various weights of calibration weights available to facilitate the collection of sensor raw data. Furthermore, multiple weights of the same weight can be utilized to collect raw data for multiple touches. To standardize the input and output of data collection, a weight map has been developed. The weight map illustrates both contact position and touch force. As demonstrated in Figure 7, each weight map's grid is mapped onto the electrode pattern. When a sensor's surface is covered with weights, the received weight map must also be represented numerically. The units of the weight map are g.

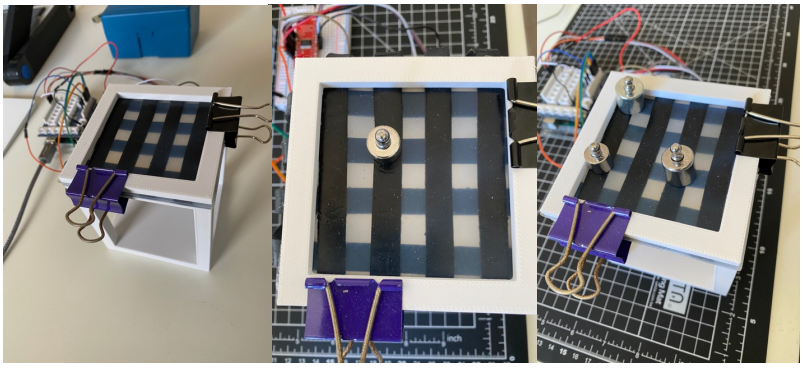

Fig. 5. Left: Weight and force collector prototype. Middle: Collect touching localization and force. Right: Collect data of multiple touching

During data collection, we placed calibration weights on the surface of the soft sensor. The weight maps were then modified based on the existing positioning and weight counts. We created a data collection script that reads unprocessed data and combines it in real-time with the weight map. Our script significantly simplifies and accelerates the data collection process. Our data script ensures that the current weight map corresponds to the actual position of the weight. In the unfortunate event that erroneous data is collected, data collection can be temporarily suspended. Each time data is collected, the script verifies its storage location and determines whether it will overwrite existing data. When it is confirmed that data collection has begun, the script will collect the necessary records automatically. When the collection is complete, the script asks if the next collection round should be initiated. To improve the quality of the data, we used the moving average to increase their stability. The logic behind the calculation of the moving average is to determine the mean of 32 records per electrode. The script automatically stores 100 records for each scenario sampled and it is capable of assembling the raw data and the weight map in a specific format. The final data set includes capacitance values, weighting plots, and moving average spans for each electrode. A single touch point with the same weight can be sampled in less than 20 minutes using the script. Currently, we can sample more than 30,00 records per data collection cycle.

Several critical tricks must be taken into account during data collection. Due to environmental factors, the initial value of the flexible sensor will vary slightly each time the data collector is powered on. This can lead to some variation in the collected data. Therefore, when we begin the data collection, we will collect the initial data from the sensor in its invariable state. During the phase of data processing, these data will be used for calibration. Additionally, because the physical state of electrodes cannot be guaranteed to be identical, the initial values of electrodes will vary slightly. When collecting the data, we must ensure that its sequence matches that of the electrodes. This will preserve the maximum amount of positional data.

4.2 3D Deformation Sampling

To generate a data set for deformation data, we need to introduce vision-based solutions. With the support of deep learning networks, motion capture systems have advanced in recent years. OptiTrack [35] is a motion capture system that primarily utilizes vision-based solutions and numerous top-tier research teams and businesses have utilized it as an industrial solution. One of OptiTrack's advantages is its ability to track the 3D positions of reflective markers

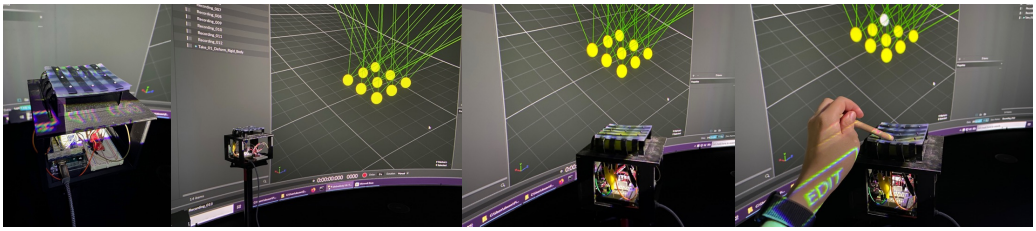

(a) (b) (c) (d)

Fig. 6. (a): Reflective markers attached on the surface. (b): Data collector with OptiTrack system. (c): The initial state of marker's position. (d): Recording the deformation of our soft sensor.

in real-time. We affixed 9 reflective markers to the surface of the soft sensor to collect information regarding its 3D deformation. The size of the mark is 3mm, and a grid layout has been assigned to these markers. In the meantime, a collection script to read and record sensor data was developed.

The sampling was performed in a laboratory equipped with 18 OptiTrack Cameras. This motion capture system is capable of capturing the 3D geography data of 3mm markers in real-time. To improve sampling precision, a black framework that reduces light reflection was designed. The framework holds our soft sensor and data reader and can be placed on top of a camera holder. During the sampling process, the OptiTrack system can record 120 frames per second and identify unique markers. After sampling, we merged the sensor raw data with the 3D geography data and the timestamp.

As demonstrated in Figure 6, the motion capture system can label the captured markers on a large screen. When the marker's dot transitions from yellow to white, its position information is lost. During the sampling, we must be aware of the marker status on the screen. Each segment is sampled between 1 and 2 minutes to minimize marker loss. Additionally, we must be concerned about the number of cameras that are simultaneously tracking the markers. The quantity of cameras is not always optimal. When there are too many cameras, the camera at the farthest distance frequently loses track of the marker's location. Therefore, we limit the number of cameras to four. When the acquisition begins, the data collection script is executed first and will log the sensor's current capacitance values. The motion capture system begins tracking the marker's position in real-time once the script has been executed. We will use a wooden stick to touch the surface of the sensor. The change in position of the marker is recorded and displayed in real-time on the screen. It is easy to miss the reflective markers during acquisition due to their small size. Once an obstruction is encountered, the sampling process must be repeated. Consequently, the collector is required to be aware of the movements. The duration of the acquisition process was approximately 1.5 hours. Typically, a single round of acquisition yields 48k 3D position records.

4.3 Pre-validation

After data collection, we must verify the accuracy of the collected data. For a data-driven approach, the minimum performance of the following deep learning model is determined by the data set's accuracy. A valid and clean data set simplifies the process of model debugging and improves the model's precision. Not all data collected are valid due to the external environment. Occasionally, there are biased or invalid data among the collected records. Such incorrect data can significantly reduce the accuracy and validity of the model. Therefore, additional validation is required to figure out whether or not it can be used to build a data set.

As illustrated in Figures 7 and 8, 2D touch and 3D deformation data are validated beforehand. A deep learning model has been pre-trained to support the pre-validation. When performing the pre-validation, sampled data is fed into a pre-trained model. The model will forecast a weight map based on the entered data. At this time, the accuracy of the predicted weight map is not a major concern. It is essential to determine whether there are significant deviations from the predicted weight map. In most cases, we visualize the predicted weight map. By comparing the weight map, it is possible to identify whether there are significant positional errors. In addition, if the predicted weight map significantly differs in value, the sampling procedure is reevaluated to determine if an operational error has occurred. For 3D deformation sampling, a similar pre-validation is utilized. The gap is that we apply another unique pre-trained model, FCN-P, which is trained for 3D deformation capture. The visualization graph for prediction validation is a 3D geometric graph.

5 COMPUTATION APPROACH

5.1 Data Processing

Before using the data set to train the deep learning model, the data quality must be enhanced. The initial step is to standardize the raw sensor data. Since the capacitance value of the soft sensor varies during surface deformation, we want the learning process to emphasize value variation. Therefore, the sensor data must be normalized by comparing the initial state to the changing state. As a result of the sampling process, we can obtain the capacitance value during the initial state, which is then utilized to generate the normalized sensor data. During the second step, sensor data is located using an electrode grid. Due to the fabrication process, the initial state value of each electrode varies slightly. Both the weight map data set and the 3D geography data set must be converted to the same electrode order. Therefore, the positional information can be mapped.

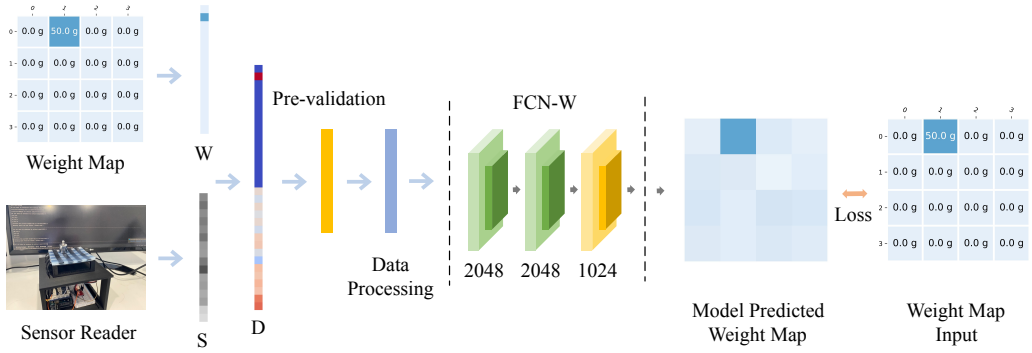

Fig. 7. Left to right: the data collection and training process of the FCN-W (Fully Connected Network) model. W is the vectorized input for the weight map, and S is the vectorized input for the sensor capacitance. Before becoming the FCN-W model's input, the data set D will undergo pre-validation and data processing. We evaluate the model's performance by measuring the loss between the predicted output and the actual input.

For the 3D geographic data, additional processing steps are required. The first step of the process is to sort the 3D geography data. Multiple rounds of raw data collection were conducted by the OptiTrack system. For each sampling workflow, the OptiTrack system will assign reflective markers a random identifier. Therefore, we must reorganize the order of the 3D geography data makers. This was achieved by analyzing the 2D geographic data. During the deformation, the vertical direction has changed significantly relative to the horizontal plane. Using the marker's grid layout, we can

quickly locate the position data. Converting Cartesian coordinates to Laplacian coordinates is another necessary step. Laplacian coordinates are widely used for surface deformation and three-dimensional mesh deformation. Laplacian coordinates, as opposed to cartesian coordinates, emphasize the relative relationship between closed pinpoints. By converting the unprocessed data set to laplacian coordinates, we can eliminate the impact of orientation and angles. To obtain laplacian coordinates, the neighboring points of each marker must be specified. Based on the visual representation of 3D geography data, we observed that the X-axis and Z-axis plane has a stable change, and we can use the relative position on the 2D plane to define neighbors. The entire data set's Laplacian coordinates were then generated utilizing the neighbors mapping.

All data processing operations are performed by developed scripts. For data processing, only the file paths and target paths of the files must be modified manually. Before using them for normalization, the script calculates the initial values of each sample. The only operation that requires human intervention is the arrangement of 3D coordinates. This step requires an inspection of the current data visualization.

5.2 Model Architecture

Our model architecture aims to reflect the real-time surface change of our soft sensor. Two lightweights, fully connected neural networks (FCN) are used to construct this capability. Sensor electrode capacitances S are the input data set for both FCN models. During data processing, each input data $S \in \mathbb{R}^{16}$ is normalized and can be used for two FCN models simultaneously. For touching force and contact localization, we map each input data S to a weight map output $W \in \mathbb{R}^{16}$ using the FCN model (FCN-W). As described in the section on data collection, the weight map W contains the weight of the touching force and location. For the deformation tracking, we employ an additional FCN model (FCN-P) that maps sensor data input S to marker positions with laplacian coordinates $P \in \mathbb{R}^{3\times M}$. M is the number of markers, which is nine, and P represents the relative positions between markers.

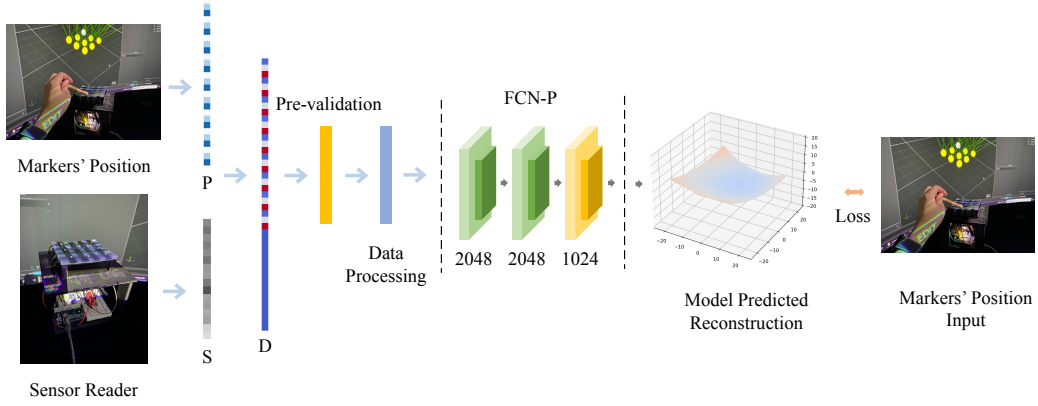

Fig. 8. Left to right: the FCN-P model's data collection and training processes. P is the vectorized input for the 3D location of reflective marks, and S is the vectorized input for the sensor capacitance. D represents the merged data set records by timestamp. We enhance the performance of the model by decreasing the distance between the predicted marker locations and the actual input.

Figure 7 and Figure 8 depict the network architecture of the FCN-W and FCN-P models. FCN-W and FCN-P both include a 16-unit input layer. The input layer is followed by three fully interconnected hidden layers in the FCN-W model. Each of the first two hidden layers contains 2048 units, while the third and final hidden layer has 1048 units. The

final output layer includes 16 units that predict the weight map values. Following all hidden layers and the input layer is the ReLu activation function. FCN-P shares the same architecture as FCN-W with the exception of the output layer. 27 units reflect the predicted position P in the output layer of FCN-P.

PyTorch is used to implement the FCN-W and FCN-P models. Both models are trained with squared L^2 loss. For both models, we use the ADAM optimizer with a learning rate of 10^{-3} and weight decay of 10^{-5}. During the process of network model training, the batch size of two network models is 64. FCN-W was trained for 20 epochs and FCN-P for 4 epochs.

6 TASK EVALUATION

To validate the utility of our soft sensor, we design and collect data sets from various scenarios. In our experiment, we use a model that has been trained with data from every possible scenario. For each scenario, we reserve one set of data for testing purposes. This enables us to compare the accuracy of various scenarios. Figure 11 illustrates the integrated soft sensor and data reader that we use to conduct our experiments. The framework is 3D-printed, and the sensor is linked to an Arduino-based data reader.

To deploy the trained models, an application script that can read sensor data and load trained models in real-time is implemented. After training, our application script can reconstruct out-of-sight deformation without a vision-based solution. After being initiated, the reading function of our application script will continue to collect sensor raw data in milliseconds. The raw data will be sorted and normalized into the proper format as input data $S \in \mathbb{R}^{16}$. The regressing function will load the same input into FCN-W and FCN-P models that have been trained. After the prediction, we can obtain the current weight map $W \in \mathbb{R}^{16}$ and the real-time 3D position $P \in \mathbb{R}^{3\times9}$ of nine markers. The outcome of W and P will be visualized as images.

6.1 Contact Localization and Force Detection

The prototype and the data set are validated in two ways. First, our data set includes test data that can be used to evaluate the training model's accuracy. Second, to validate the generalisability of the model, we conduct experimental tests with the constructed prototype system and calibration weights on various scenarios. Figure 9 depicts that the test scenarios include four distinct sections: 50 g single-touch, 50 g multi-touch, 100 g single-touch, and 100 g multi-touch. Using the data collection script, we were able to collect information on the various scenarios within 30 minutes. Due to a large number of possible multi-touch combinations, 22 patterns were selected for the multi-touch weight map. Then, information was gathered regarding these 22 multi-touch patterns. The entire data collection process took approximately 1 hour and 15 minutes and the newly collected data were used to train our models. Training can be completed in less than 10 minutes using an automation script. Using the test data as measurements, our prototype predicted the location of the touch with 100 percent of accuracy. The average error in touch weight measurement is 2.29 g. And by visualizing the prediction results, it is clear that as the touch force increases, the capacitance of the flexible sensor increases proportionally.

For the detection of generalization ability, we utilized calibrated weights and a prototype system. Figure 11 illustrates that the prototype system can detect the position and weight of weights placed on the flexible sensor in real-time. To increase the system's stability in the prototype, moving averaging is used to filter the input data. 20 rounds of generalization tests were conducted under these conditions. The system was able to predict 100 percent of the 2D position information of the touch. The average measurement error for touch force was 5.6 g. The maximum error was 12.9 g and the smallest error was 0.2 grams. In addition, it was discovered that increasing the moving averaging time

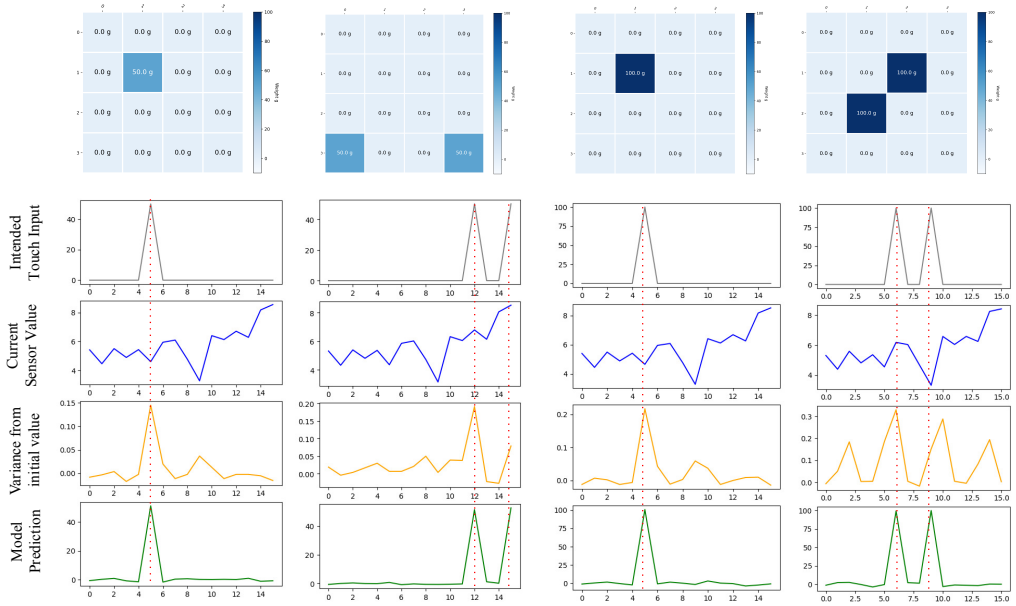

Fig. 9. From left to right, there are four distinct weight maps: 50g single-touch, 50g multi-touch, 100g single-touch, and 100g multi-touch. From top to bottom are arranged the vectorized weight map, the capacitance value of the sensor, the change in capacitance value, and the predicted value after training. The dashed lines depict the quantitative relationship between touch position and sensor data.

to 3 seconds significantly decreased the maximum error. During the generalization test, we noticed that the weight's position affected the final weight value. The position is closer to the electrodes when the error in the final weight value is smaller. In addition, we trained fine-tuned models for each test scenario. The average error in the generalization test was reduced with the tuned model.

6.2 3D Deformation Capture

To test the ability of deformation capture in real-time, we have developed a real-time system that can analyze sensor signals as well as able to perform the three-dimensional reconstruction. Our real-time system initiation does not require vision equipment. As shown in Figure 11, the system will display the reconstructed surface. When a wooden stick is pressed against the sensor, the reconstructed plane also deforms in real-time. To reveal the deformation, two virtual planes with separate subdivision parameters are selected. Due to size limitations, the vertical displacement is greater than the horizontal displacement when deformation occurs. As described in Figure 10, the variation in the vertical direction of the marker can correspond to the variation in capacitance of the sensor. Our system prototype synchronizes deformation with a delay of approximately 1 second.

Due to the coordinate transformation, it is tricky to visually determine the position of the 3D reconstruction plane. Consequently, we utilize the test data set for accuracy checks. After training, our model can predict the 3D geographic data for each marker. The trained model has an average loss of 1.66, compared to 1.34 for a random sample of test data. Noting that 3D location training can easily result in overfitting, care should be taken when adjusting the model's

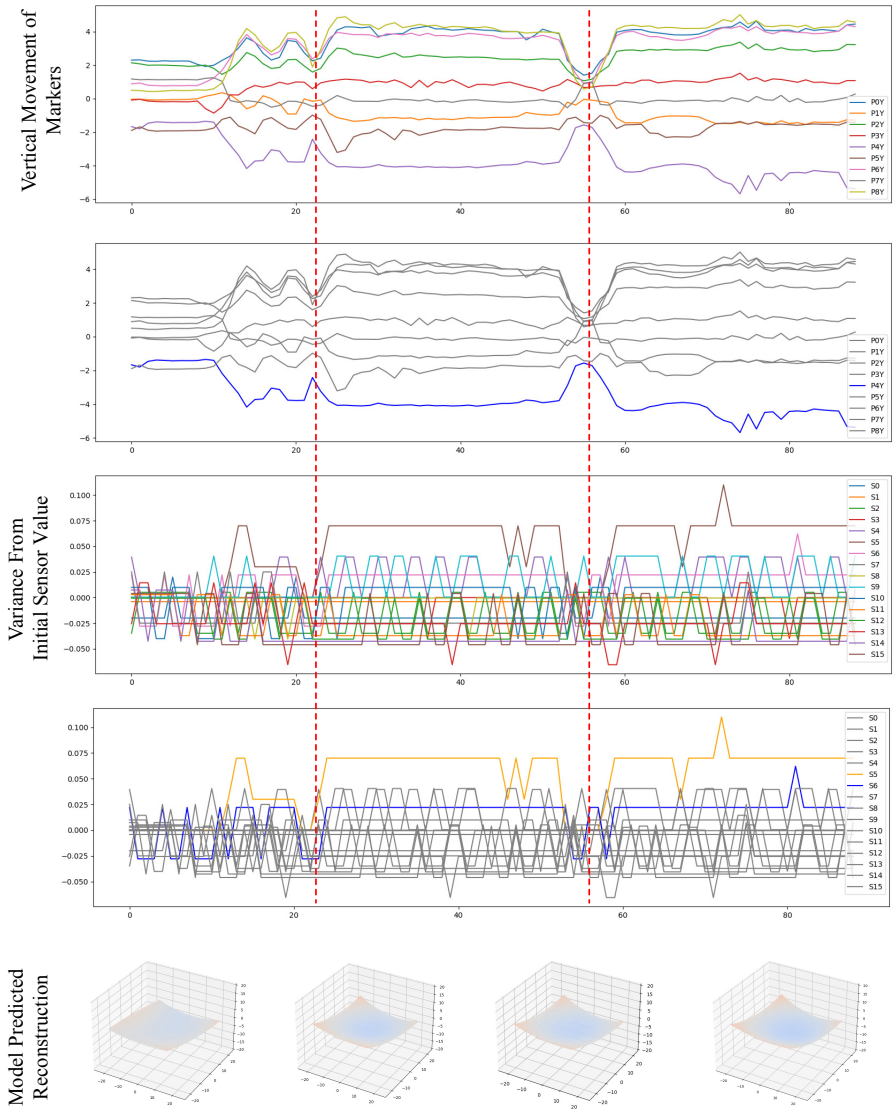

Fig. 10. The two images at the top illustrate the change in vertical position of markers during deformation. The second graph highlights the vertical position route of the central marker. In the two middle plots, the the corresponding sensor capacitance variance values are represented. Changes in the electrodes adjacent to the central marker are highlighted. The 3D-reconstructed plane, predicted by our prototype system, is located at the base of the image. The dashed line displays the relationship between the vertical position of the marker and the capacitance variation.

fine-tuned parameters. In the test for generalizability, pressing on the edges causes significantly less deformation than pressing in the center. This is because the edges of the sensor prototype are supported by a rigid frame, which leads to

less data deformation. Figure 11 demonstrates that even in the absence of light or presence of occlusion, the prototype system is capable of reconstructing the surface's deformation in real-time.

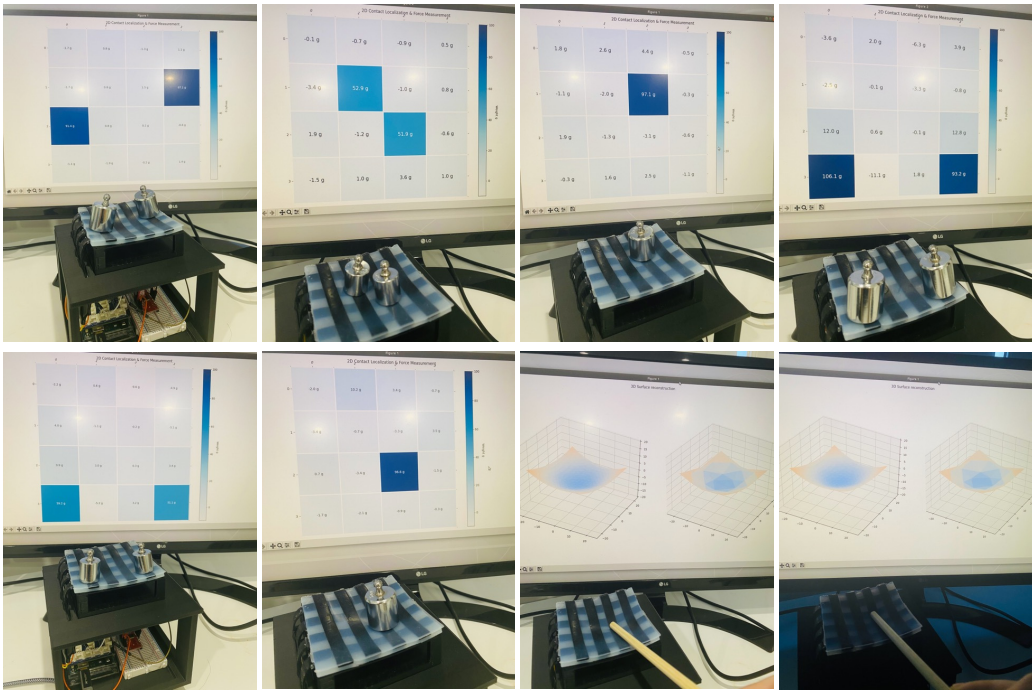

Fig. 11. A gallery of use cases for real-time soft sensor systems. It includes single-point and multiple-point touching detection, 3D deformation reconstruction, and detection of deformation in darkness.

7 CONCLUSION AND FUTURE WORK

In this paper, we present a novel low-cost soft sensor. In addition, a high-quality soft sensor must be inexpensive to fabricate, simple to install, and effective. We achieve these goals through several contributions, including the design of the sensor layout, the selection of materials, the automation of the manufacturing process using 3D printers and laser cutters, the development of an Arduino-based readout solution, an efficient data collection process and the creation of new data-driven models. We validated the accuracy of the new dataset using a live prototype system based on our soft sensor. Experiments with various scenarios demonstrate that the data-driven model is generalizable.

For future research, we would like to extend the usage of our soft senor by detecting the surface deformation of 3D objects. It can be accomplished by attaching multiple soft sensors to the surface of a large 3D object. This objective will present additional challenges, such as mapping 2D deformation to 3D objects. Consequently, we intend to improve the electrode arrangement. A triangular structure of the electrode layout is more resistant to deformation than a grid structure, and a triangular mesh layout, which has been used in 3D reconstruction as a mesh pattern, can decrease the complexity of mapping 2D to 3D. In addition, we wish to increase the sensor size and number of electrodes by modernizing the fabrication process. This will allow large object surface deformations to be detected. Furthermore, we expect to develop appropriate data-driven models for the enormous quantity of raw data generated by the triangular

layout. The accomplishment of these research objectives will significantly expand the scope of use cases for our sensors. For instance, it could be used to detect industrial product deformation in situations where camera performance is limited.

REFERENCES

[1] Jason Alexander, Anne Roudaut, Jürgen Steimle, Kasper Hornbæk, Miguel Bruns Alonso, Sean Follmer, and Timothy Merritt. 2018. Grand Challenges in Shape-Changing Interface Research. In *Proceedings of the 2018 CHI Conference on Human Factors in Computing Systems* (Montreal QC, Canada) *(CHI '18)*. Association for Computing Machinery, New York, NY, USA, 1–14. https://doi.org/10.1145/3173574.3173873

[2] Oluwaseun Araromi, Samuel Rosset, and Herbert Shea. 2015. High-Resolution, Large-Area Fabrication of Compliant Electrodes via Laser Ablation for Robust, Stretchable Dielectric Elastomer Actuators and Sensors. *ACS applied materials & interfaces* 7 (07 2015). https://doi.org/10.1021/acsami.5b04975

[3] Moritz Bächer, Benjamin Hepp, Fabrizio Pece, Paul G. Kry, Bernd Bickel, Bernhard Thomaszewski, and Otmar Hilliges. 2016. DefSense: Computational Design of Customized Deformable Input Devices. In *Proceedings of the 2016 CHI Conference on Human Factors in Computing Systems* (San Jose, California, USA) *(CHI '16)*. Association for Computing Machinery, New York, NY, USA, 3806–3816. https://doi.org/10.1145/2858036.2858354

[4] Rebecca Baldwin, Stan Bobovych, Ryan Robucci, Chintan Patel, and Nilanjan Banerjee. 2015. Gait Analysis for Fall Prediction Using Hierarchical Textile-Based Capacitive Sensor Arrays. In *Proceedings of the 2015 Design, Automation Test in Europe Conference Exhibition* (Grenoble, France) *(DATE '15)*. EDA Consortium, San Jose, CA, USA, 1293–1298.

[5] Alberto Boem. 2014. Sculpton: A malleable tangible interface for sound sculpting. In *Proceedings of the 2014 Joint International Computer Music Conference and Sound and Music Computing, ICMA 2014, San Francisco, USA, 2014*. Michigan Publishing. https://quod.lib.umich.edu/i/icmc/bbp2372.2014.115/1

[6] Alberto Boem and Giovanni Maria Troiano. 2019. Non-Rigid HCI: A Review of Deformable Interfaces and Input. In *Proceedings of the 2019 on Designing Interactive Systems Conference* (San Diego, CA, USA) *(DIS '19)*. Association for Computing Machinery, New York, NY, USA, 885–906. https://doi.org/10.1145/3322276.3322347

[7] R. Chatterjee and F. Matsuno. 2008. Capacitive touch sensor based user-interface : Generic design considerations and development of an wearable input device. In *2008 SICE Annual Conference*. 2299–2303. https://doi.org/10.1109/SICE.2008.4655048

[8] Eshwar Reddy Cholleti, Jonathan Stringer, Mahtab Assadian, Virginie Battmann, Chris Bowen, and Kean Aw. 2019. Highly Stretchable Capacitive Sensor with Printed Carbon Black Electrodes on Barium Titanate Elastomer Composite. *Sensors* 19, 1 (2019). https://doi.org/10.3390/s19010042

[9] Gabe Cohn, Sidhant Gupta, Tien-Jui Lee, Dan Morris, Joshua R. Smith, Matthew S. Reynolds, Desney S. Tan, and Shwetak N. Patel. 2012. An Ultra-Low-Power Human Body Motion Sensor Using Static Electric Field Sensing. In *Proceedings of the 2012 ACM Conference on Ubiquitous Computing* (Pittsburgh, Pennsylvania) *(UbiComp '12)*. Association for Computing Machinery, New York, NY, USA, 99–102. https://doi.org/10.1145/2370216.2370233

[10] Gabe Cohn, Daniel Morris, Shwetak Patel, and Desney Tan. 2012. Humantenna: Using the Body as an Antenna for Real-Time Whole-Body Interaction. In *Proceedings of the SIGCHI Conference on Human Factors in Computing Systems* (Austin, Texas, USA) *(CHI '12)*. Association for Computing Machinery, New York, NY, USA, 1901–1910. https://doi.org/10.1145/2207676.2208330

[11] Elkem. [n.d.]. *Elkem Medical Grade RTV Silicone*. https://www.elkem.com/silicones/offer/healthcare/medical-grade/room-temperature-vulcanizing/

[12] Oliver Glauser, Daniele Panozzo, Otmar Hilliges, and Olga Sorkine-Hornung. 2019. Deformation Capture via Soft and Stretchable Sensor Arrays. *ACM Trans. Graph.* 38, 2, Article 16 (mar 2019), 16 pages. https://doi.org/10.1145/3311972

[13] Oliver Glauser, Shihao Wu, Daniele Panozzo, Otmar Hilliges, and Olga Sorkine-Hornung. 2019. Interactive Hand Pose Estimation Using a Stretch-Sensing Soft Glove. *ACM Trans. Graph.* 38, 4, Article 41 (jul 2019), 15 pages. https://doi.org/10.1145/3306346.3322957

[14] Nan-Wei Gong, Jürgen Steimle, Simon Olberding, Steve Hodges, Nicholas Edward Gillian, Yoshihiro Kawahara, and Joseph A. Paradiso. 2014. PrintSense: A Versatile Sensing Technique to Support Multimodal Flexible Surface Interaction. In *Proceedings of the SIGCHI Conference on Human Factors in Computing Systems* (Toronto, Ontario, Canada) *(CHI '14)*. Association for Computing Machinery, New York, NY, USA, 1407–1410. https://doi.org/10.1145/2556288.2557173

[15] Tobias Grosse-Puppendahl, Yannick Berghoefer, Andreas Braun, Raphael Wimmer, and Arjan Kuijper. 2013. OpenCapSense: A rapid prototyping toolkit for pervasive interaction using capacitive sensing. In *2013 IEEE International Conference on Pervasive Computing and Communications (PerCom)*. 152–159. https://doi.org/10.1109/PerCom.2013.6526726

[16] Tobias Grosse-Puppendahl, Christian Holz, Gabe Cohn, Raphael Wimmer, Oskar Bechtold, Steve Hodges, Matthew S. Reynolds, and Joshua R. Smith. 2017. Finding Common Ground: A Survey of Capacitive Sensing in Human-Computer Interaction. In *Proceedings of the 2017 CHI Conference on Human Factors in Computing Systems* (Denver, Colorado, USA) *(CHI '17)*. Association for Computing Machinery, New York, NY, USA, 3293–3315. https://doi.org/10.1145/3025453.3025808

[17] Jaehyun Han, Jiseong Gu, and Geehyuk Lee. 2014. Trampoline: A Double-Sided Elastic Touch Device for Creating Reliefs. In *Proceedings of the 27th Annual ACM Symposium on User Interface Software and Technology* (Honolulu, Hawaii, USA) *(UIST '14)*. Association for Computing Machinery, New York, NY, USA, 383–388. https://doi.org/10.1145/2642918.2647381

[18] Ken Hinckley and Mike Sinclair. 1999. Touch-Sensing Input Devices. In *Proceedings of the SIGCHI Conference on Human Factors in Computing Systems* (Pittsburgh, Pennsylvania, USA) *(CHI '99)*. Association for Computing Machinery, New York, NY, USA, 223–230. https://doi.org/10.1145/302979.303045

[19] Bo Huang, Mingyu Li, Tao Mei, David McCoul, Shihao Qin, Zhanfeng Zhao, and Jianwen Zhao. 2017. Wearable Stretch Sensors for Motion Measurement of the Wrist Joint Based on Dielectric Elastomers. *Sensors* 17, 12 (2017). https://doi.org/10.3390/s17122708

[20] Joseph A Paradiso Irmandy Wicaksono. 2017. FabricKeyboard: Multimodal Textile Sensate Media as an Expressive and Deformable Musical Interface. In *NIME'17*. Aalborg University Copenhagen, 348–353.

[21] Heijun Jeong and Sungjoon Lim. 2016. A Stretchable Radio-Frequency Strain Sensor Using Screen Printing Technology. *Sensors* 16, 11 (2016). https://doi.org/10.3390/s16111839

[22] Hsin-Liu (Cindy) Kao, Christian Holz, Asta Roseway, Andres Calvo, and Chris Schmandt. 2016. DuoSkin: Rapidly Prototyping on-Skin User Interfaces Using Skin-Friendly Materials. In *Proceedings of the 2016 ACM International Symposium on Wearable Computers* (Heidelberg, Germany) *(ISWC '16)*. Association for Computing Machinery, New York, NY, USA, 16–23. https://doi.org/10.1145/2971763.2971777

[23] Gierad Laput, Chouchang Yang, Robert Xiao, Alanson Sample, and Chris Harrison. 2015. EM-Sense: Touch Recognition of Uninstrumented, Electrical and Electromechanical Objects. In *Proceedings of the 28th Annual ACM Symposium on User Interface Software & Technology* (Charlotte, NC, USA) *(UIST '15)*. Association for Computing Machinery, New York, NY, USA, 157–166. https://doi.org/10.1145/2807442.2807481

[24] Chris Larson, Josef Spjut, Ross Knepper, and Robert Shepherd. 2019. A Deformable Interface for Human Touch Recognition Using Stretchable Carbon Nanotube Dielectric Elastomer Sensors and Deep Neural Networks. *Soft Robotics* 6, 5 (2019), 611–620. https://doi.org/10.1089/soro.2018.0086 arXiv:https://doi.org/10.1089/soro.2018.0086 PMID: 31381482.

[25] Mathieu Le Goc, Stuart Taylor, Shahram Izadi, and Cem Keskin. 2014. A Low-Cost Transparent Electric Field Sensor for 3d Interaction on Mobile Devices. In *Proceedings of the SIGCHI Conference on Human Factors in Computing Systems* (Toronto, Ontario, Canada) *(CHI '14)*. Association for Computing Machinery, New York, NY, USA, 3167–3170. https://doi.org/10.1145/2556288.2557331

[26] Roman Lissermann, Jochen Huber, Aristotelis Hadjakos, Suranga Nanayakkara, and Max Mühlhäuser. 2014. EarPut: Augmenting Ear-Worn Devices for Ear-Based Interaction. In *Proceedings of the 26th Australian Computer-Human Interaction Conference on Designing Futures: The Future of Design* (Sydney, New South Wales, Australia) *(OzCHI '14)*. Association for Computing Machinery, New York, NY, USA, 300–307. https://doi.org/10.1145/2686612.2686655

[27] Xingxing Ma, Jiajie Guo, Kok-Meng Lee, Luye Yang, and Minghui Chen. 2019. A Soft Capacitive Wearable Sensing System for Lower-Limb Motion Monitoring. In *Intelligent Robotics and Applications: 12th International Conference, ICIRA 2019, Shenyang, China, August 8–11, 2019, Proceedings, Part IV* (Shenyang, China). Springer-Verlag, Berlin, Heidelberg, 467–479. https://doi.org/10.1007/978-3-030-27538-9_40

[28] Brian Mayton, Louis LeGrand, and Joshua R. Smith. 2010. An Electric Field Pretouch system for grasping and co-manipulation. In *2010 IEEE International Conference on Robotics and Automation*. 831–838. https://doi.org/10.1109/ROBOT.2010.5509658

[29] Andreas Mehmann, Matija Varga, Karl Gönner, and Gerhard Tröster. 2015. A Ball-Grid-Array-like Electronics-to-Textile Pocket Connector for Wearable Electronics. In *Proceedings of the 2015 ACM International Symposium on Wearable Computers* (Osaka, Japan) *(ISWC '15)*. Association for Computing Machinery, New York, NY, USA, 57–60. https://doi.org/10.1145/2802083.2802093

[30] Mohammad Faizuddin Mohd Noor, Andrew Ramsay, Stephen Hughes, Simon Rogers, John Williamson, and Roderick Murray-Smith. 2014. 28 Frames Later: Predicting Screen Touches from Back-of-Device Grip Changes. In *Proceedings of the SIGCHI Conference on Human Factors in Computing Systems* (Toronto, Ontario, Canada) *(CHI '14)*. Association for Computing Machinery, New York, NY, USA, 2005–2008. https://doi.org/10.1145/2556288.2557148

[31] T Murakami and N Nakajima. 2000. DO-IT: deformable object as input tool for 3-D geometric operation. *Computer-Aided Design* 32, 1 (2000), 5–16. https://doi.org/10.1016/S0010-4485(99)00078-0

[32] Ken Nakagaki, Luke Vink, Jared Counts, Daniel Windham, Daniel Leithinger, Sean Follmer, and Hiroshi Ishii. 2016. Materiable: Rendering Dynamic Material Properties in Response to Direct Physical Touch with Shape Changing Interfaces. In *Proceedings of the 2016 CHI Conference on Human Factors in Computing Systems* (San Jose, California, USA) *(CHI '16)*. Association for Computing Machinery, New York, NY, USA, 2764–2772. https://doi.org/10.1145/2858036.2858104

[33] Vinh P. Nguyen, Sang Ho Yoon, Ansh Verma, and Karthik Ramani. 2014. BendID: Flexible Interface for Localized Deformation Recognition. In *Proceedings of the 2014 ACM International Joint Conference on Pervasive and Ubiquitous Computing* (Seattle, Washington) *(UbiComp '14)*. Association for Computing Machinery, New York, NY, USA, 553–557. https://doi.org/10.1145/2632048.2636092

[34] Jaime Oliver and Mathew Jenkins. 2008. The Silent Drum controller: a New percussive gestural Interface. In *Proceedings of the 2008 International Computer Music Conference, ICMC 2008, Belfast, Ireland, August 24-29, 2008*. Michigan Publishing. https://hdl.handle.net/2027/spo.bbp2372.2008.118

[35] OptiTrack. [n.d.]. *OptiTrack - Motion Capture Systems*. https://optitrack.com/

[36] Patrick Parzer, Kathrin Probst, Teo Babic, Christian Rendl, Anita Vogl, Alex Olwal, and Michael Haller. 2016. FlexTiles: A Flexible, Stretchable, Formable, Pressure-Sensitive, Tactile Input Sensor. In *Proceedings of the 2016 CHI Conference Extended Abstracts on Human Factors in Computing Systems* (San Jose, California, USA) *(CHI EA '16)*. Association for Computing Machinery, New York, NY, USA, 3754–3757. https://doi.org/10.1145/2851581.2890253

[37] Patrick Parzer, Adwait Sharma, Anita Vogl, Jürgen Steimle, Alex Olwal, and Michael Haller. 2017. SmartSleeve: Real-Time Sensing of Surface and Deformation Gestures on Flexible, Interactive Textiles, Using a Hybrid Gesture Detection Pipeline. In *Proceedings of the 30th Annual ACM Symposium on User Interface Software and Technology* (Québec City, QC, Canada) *(UIST '17)*. Association for Computing Machinery, New York, NY, USA, 565–577. https://doi.org/10.1145/3126594.3126652

[38] Huaishu Peng, Jennifer Mankoff, Scott E. Hudson, and James McCann. 2015. A Layered Fabric 3D Printer for Soft Interactive Objects. In *Proceedings of the 33rd Annual ACM Conference on Human Factors in Computing Systems* (Seoul, Republic of Korea) *(CHI '15)*. Association for Computing Machinery, New York, NY, USA, 1789–1798. https://doi.org/10.1145/2702123.2702327

[39] Majken K. Rasmussen, Esben W. Pedersen, Marianne G. Petersen, and Kasper Hornbæk. 2012. Shape-Changing Interfaces: A Review of the Design Space and Open Research Questions. In *Proceedings of the SIGCHI Conference on Human Factors in Computing Systems* (Austin, Texas, USA) *(CHI '12)*. Association for Computing Machinery, New York, NY, USA, 735–744. https://doi.org/10.1145/2207676.2207781

[40] Jun Rekimoto. 2002. SmartSkin: An Infrastructure for Freehand Manipulation on Interactive Surfaces. In *Proceedings of the SIGCHI Conference on Human Factors in Computing Systems* (Minneapolis, Minnesota, USA) *(CHI '02)*. Association for Computing Machinery, New York, NY, USA, 113–120. https://doi.org/10.1145/503376.503397

[41] Christian Rendl, Patrick Greindl, Michael Haller, Martin Zirkl, Barbara Stadlober, and Paul Hartmann. 2012. *PyzoFlex: Printed Piezoelectric Pressure Sensing Foil*. Association for Computing Machinery, New York, NY, USA, 509–518. https://doi.org/10.1145/2380116.2380180

[42] Christian Rendl, David Kim, Sean Fanello, Patrick Parzer, Christoph Rhemann, Jonathan Taylor, Martin Zirkl, Gregor Scheipl, Thomas Rothländer, Michael Haller, and Shahram Izadi. 2014. FlexSense: A Transparent Self-Sensing Deformable Surface. In *Proceedings of the 27th Annual ACM Symposium on User Interface Software & Technology* (Honolulu, Hawaii, USA) *(UIST '14)*. Association for Computing Machinery, New York, NY, USA, 129–138. https://doi.org/10.1145/2642918.2647405

[43] Samuel Rosset, Oluwaseun A Araromi, Samuel Schlatter, and Herbert R Shea. 2016. Fabrication process of silicone-based dielectric elastomer actuators. *JoVE (Journal of Visualized Experiments)* 108 (2016), e53423.

[44] A. Roudaut, D. Krusteva, M. McCoy, A. Karnik, K Ramani, and S. Subramanian. 2016. Cubimorph: Designing modular interactive devices. In *2016 IEEE International Conference on Robotics and Automation (ICRA)*. 3339–3345. https://doi.org/10.1109/ICRA.2016.7487508

[45] Silvia Rus, Tobias Grosse-Puppendahl, and Arjan Kuijper. 2014. Recognition of bed postures using mutual capacitance sensing. In *European Conference on Ambient Intelligence*. Springer, 51–66.

[46] Silvia Rus, Tobias Grosse-Puppendahl, and Arjan Kuijper. 2017. Evaluating the Recognition of Bed Postures Using Mutual Capacitance Sensing. *J. Ambient Intell. Smart Environ.* 9, 1 (jan 2017), 113–127. https://doi.org/10.3233/AIS-160414

[47] Mirza Saquib Sarwar, Yuta Dobashi, Claire Preston, Justin K. M. Wyss, Shahriar Mirabbasi, and John David Wyndham Madden. 2017. Bend, stretch, and touch: Locating a finger on an actively deformed transparent sensor array. *Science Advances* 3, 3 (2017), e1602200. https://doi.org/10.1126/sciadv.1602200 arXiv:https://www.science.org/doi/pdf/10.1126/sciadv.1602200

[48] Valkyrie Savage, Xiaohan Zhang, and Björn Hartmann. 2012. *Midas: Fabricating Custom Capacitive Touch Sensors to Prototype Interactive Objects*. Association for Computing Machinery, New York, NY, USA, 579–588. https://doi.org/10.1145/2380116.2380189

[49] Martin Schmitz, Mohammadreza Khalilbeigi, Matthias Balwierz, Roman Lissermann, Max Mühlhäuser, and Jürgen Steimle. 2015. Capricate: A Fabrication Pipeline to Design and 3D Print Capacitive Touch Sensors for Interactive Objects. In *Proceedings of the 28th Annual ACM Symposium on User Interface Software & Technology* (Charlotte, NC, USA) *(UIST '15)*. Association for Computing Machinery, New York, NY, USA, 253–258. https://doi.org/10.1145/2807442.2807503

[50] Tsuyoshi Sekitani, Hiroyoshi Nakajima, Hiroki Maeda, Takanori Fukushima, Takuzo Aida, Kenji Hata, and Takao Someya. 2009. Stretchable active-matrix organic light-emitting diode display using printable elastic conductors. *Nature materials* 8, 6 (2009), 494–499.

[51] Gurashish Singh, Alexander Nelson, Ryan Robucci, Chintan Patel, and Nilanjan Banerjee. 2015. Inviz: Low-power personalized gesture recognition using wearable textile capacitive sensor arrays. In *2015 IEEE International Conference on Pervasive Computing and Communications (PerCom)*. 198–206. https://doi.org/10.1109/PERCOM.2015.7146529

[52] Jürgen Steimle, Andreas Jordt, and Pattie Maes. 2013. Flexpad: Highly Flexible Bending Interactions for Projected Handheld Displays. In *Proceedings of the SIGCHI Conference on Human Factors in Computing Systems* (Paris, France) *(CHI '13)*. Association for Computing Machinery, New York, NY, USA, 237–246. https://doi.org/10.1145/2470654.2470688

[53] Stratasys. [n.d.]. *Industrial 3D Printing & Additive Manufacturing - Stratasys*. https://www.stratasys.com/en/

[54] Yuta Sugiura, Masahiko Inami, and Takeo Igarashi. 2012. *A Thin Stretchable Interface for Tangential Force Measurement*. Association for Computing Machinery, New York, NY, USA, 529–536. https://doi.org/10.1145/2380116.2380182

[55] Koray Tahiroğlu, Thomas Svedström, Valtteri Wikström, Simon Overstall, Johan Kildal, and Teemu Ahmaniemi. 2014. SoundFLEX: Designing Audio to Guide Interactions with Shape-Retaining Deformable Interfaces. In *Proceedings of the 16th International Conference on Multimodal Interaction* (Istanbul, Turkey) *(ICMI '14)*. Association for Computing Machinery, New York, NY, USA, 267–274. https://doi.org/10.1145/2663204.2663278

[56] Giovanni Maria Troiano, Esben Warming Pedersen, and Kasper Hornbæk. 2015. Deformable Interfaces for Performing Music. In *Proceedings of the 33rd Annual ACM Conference on Human Factors in Computing Systems* (Seoul, Republic of Korea) *(CHI '15)*. Association for Computing Machinery, New York, NY, USA, 377–386. https://doi.org/10.1145/2702123.2702492

[57] Tubal. [n.d.]. *TUBALL MATRIX 601*. https://tuball.com/additives/601

[58] Tomas Unander, Hans-Erik Nilsson, and Bengt Oelmann. 2007. Printed touch sensor for interactive packaging and display. In *Polytronic 2007 - 6th International Conference on Polymers and Adhesives in Microelectronics and Photonics*. 12–17. https://doi.org/10.1109/POLYTR.2007.4339128

[59] Katia Vega, Marcio Cunha, and Hugo Fuks. 2015. Hairware: The Conscious Use of Unconscious Auto-Contact Behaviors. In *Proceedings of the 20th International Conference on Intelligent User Interfaces* (Atlanta, Georgia, USA) *(IUI '15)*. Association for Computing Machinery, New York, NY, USA, 78–86. https://doi.org/10.1145/2678025.2701404

[60] Martin Weigel, Tong Lu, Gilles Bailly, Antti Oulasvirta, Carmel Majidi, and Jürgen Steimle. 2015. ISkin: Flexible, Stretchable and Visually Customizable On-Body Touch Sensors for Mobile Computing. In *Proceedings of the 33rd Annual ACM Conference on Human Factors in Computing Systems* (Seoul, Republic of Korea) *(CHI '15)*. Association for Computing Machinery, New York, NY, USA, 2991–3000. https://doi.org/10.1145/2702123.2702391

[61] Michael Wessely, Theophanis Tsandilas, and Wendy E. Mackay. 2016. Stretchis: Fabricating Highly Stretchable User Interfaces. In *Proceedings of the 29th Annual Symposium on User Interface Software and Technology* (Tokyo, Japan) *(UIST '16)*. Association for Computing Machinery, New York, NY, USA, 697–704. https://doi.org/10.1145/2984511.2984521

[62] Valtteri Wikström, Simon Overstall, Koray Tahiroğlu, Johan Kildal, and Teemu Ahmaniemi. 2013. MARSUI: Malleable Audio-Reactive Shape-Retaining User Interface. In *CHI '13 Extended Abstracts on Human Factors in Computing Systems* (Paris, France) *(CHI EA '13)*. Association for Computing Machinery, New York, NY, USA, 3151–3154. https://doi.org/10.1145/2468356.2479633

[63] Raphael Wimmer, Matthias Kranz, Sebastian Boring, and Albrecht Schmidt. 2007. A Capacitive Sensing Toolkit for Pervasive Activity Detection and Recognition. In *Fifth Annual IEEE International Conference on Pervasive Computing and Communications (PerCom'07)*. 171–180. https://doi.org/10.1109/PERCOM.2007.1

[64] Jin Yan, Austin Downey, Alessandro Cancelli, Simon Laflamme, An Chen, Jian Li, and Filippo Ubertini. 2019. Concrete Crack Detection and Monitoring Using a Capacitive Dense Sensor Array. *Sensors* 19, 8 (2019). https://doi.org/10.3390/s19081843

[65] Doruk Yildirim, Luis Edgardo Fraguada, and Elizabeth Esther Bigger. 2019. DualSkin: Ambient Electric Field Sensing Wearable. In *Proceedings of the 23rd International Symposium on Wearable Computers* (London, United Kingdom) *(ISWC '19)*. Association for Computing Machinery, New York, NY, USA, 339–345. https://doi.org/10.1145/3341163.3346931

[66] Sang Ho Yoon, Ke Huo, Yunbo Zhang, Guiming Chen, Luis Paredes, Subramanian Chidambaram, and Karthik Ramani. 2017. ISoft: A Customizable Soft Sensor with Real-Time Continuous Contact and Stretching Sensing. In *Proceedings of the 30th Annual ACM Symposium on User Interface Software and Technology* (Québec City, QC, Canada) *(UIST '17)*. Association for Computing Machinery, New York, NY, USA, 665–678. https://doi.org/10.1145/3126594.3126654

[67] Sang Ho Yoon, Luis Paredes, Ke Huo, and Karthik Ramani. 2018. MultiSoft: Soft Sensor Enabling Real-Time Multimodal Sensing with Contact Localization and Deformation Classification. *Proc. ACM Interact. Mob. Wearable Ubiquitous Technol.* 2, 3, Article 145 (sep 2018), 21 pages. https://doi.org/10.1145/3264955